

RSC Advances



This is an *Accepted Manuscript*, which has been through the Royal Society of Chemistry peer review process and has been accepted for publication.

Accepted Manuscripts are published online shortly after acceptance, before technical editing, formatting and proof reading. Using this free service, authors can make their results available to the community, in citable form, before we publish the edited article. This *Accepted Manuscript* will be replaced by the edited, formatted and paginated article as soon as this is available.

You can find more information about *Accepted Manuscripts* in the [Information for Authors](#).

Please note that technical editing may introduce minor changes to the text and/or graphics, which may alter content. The journal's standard [Terms & Conditions](#) and the [Ethical guidelines](#) still apply. In no event shall the Royal Society of Chemistry be held responsible for any errors or omissions in this *Accepted Manuscript* or any consequences arising from the use of any information it contains.



Electronic and transport properties of graphene with grain boundaries

Jie Sun,^a Na Lin,^{a,*} Zhenyu Li,^{b,*} Hao Ren,^c Cheng Tang,^a Xian Zhao^{a,*}

Received 00th January 20xx,
Accepted 00th January 20xx

DOI: 10.1039/x0xx00000x

www.rsc.org/

To understand the effect of grain boundaries (GBs) on the electronic transport properties of graphene, we have performed first principles studies on the electronic structure and transport properties of graphene with four single GBs and two crossed GBs. Calculations indicate that the zero band gap nature of graphene is not destroyed by introducing GBs. The localized states introduced by GBs have positive contribution to the transport ability in the vicinity of the Fermi level. The transport properties across and along the GBs show an obvious discrepancy. Compared with the pristine graphene, an at least 50% current suppression is found in the transport across the GBs, while less current degradation presents along the GBs. The transports along other directions show that the transmission ability can be efficiently enhanced by avoiding the transport direction across the GBs. Moreover, the transport behavior of the crossed GB is akin to that of the transport across a single GB.

Introduction

Graphene, a two-dimensional material consisting of sp^2 -bonded carbon atoms, has attracted significant interests due to its unique physical properties and potential applications^{1,2}. Its high performance in electronic transport properties makes it the most promising material for next generation electronic device³⁻⁵. The wafer-scale graphene films used for large-scale integration can be obtained by epitaxial on SiC substrate or chemical vapor deposition (CVD) on transition metals^{6,7}. However, in both cases the obtained films are often polycrystalline and composed of multiple graphene grains stitched by grain boundaries (GBs)⁸⁻¹⁰, which are extended defects made up of non-hexagonal rings such as pentagons and heptagons^{11,12}. These defects break the lattice symmetry and are believed to have a great impact on electronic structure and transport properties of polycrystalline graphene¹³.

Early theoretical studies on electronic structure of graphene have suggested that the van Hove singularity states close to the Fermi energy exist in certain ordered GBs^{14,15}. A recent experiment well verified these peculiar states by using scanning tunneling microscopy (STM) and confirmed that the conductance around certain ordered GBs could be significantly enhanced by these states¹⁶. For the transport investigations, there is still a debate whether the GB substantially degrade the electronic transport properties of graphene. Yu et al. found

the inter-grain (across the GB) resistance largely increased compared with intra-grain (along the grain) using four-probe measurement¹³. Nevertheless, Huang et al. declared that GBs were not strongly resistive by electrical measurement¹⁷. Instead, Clark et al. measured electronic transport near specific GBs and found the grain boundary conductance is less than one-third of the bulk conductance¹⁸. The discrepancy in these findings is mainly caused by a lack of knowledge of the precise morphology of GBs for the measured samples. In spite of the fact that precise atomic configuration at the local region of a GB can be revealed by aberration corrected high-resolution transmission electron microscope (AC-HRTEM)¹⁹, the electronic transport measurement corresponding to a definite structure of GBs is still lacking.

Despite the limitation in experiment, theoretical investigations have gained some insight into graphene with GBs. Yazyev and Louie found that the transport behaviors of GBs, either high transparency or perfect reflection of charge carriers, depended on the translation vector of the two adjacent grains based on the momentum conservation²⁰. The rationality of this statement was also verified by first principles studies²¹. Vancsó et al. showed the misorientation angle of the two adjacent graphene grains and the atomic structures of the GBs were two main factors governing the transport²². In addition, Zhang et al. predicted that the transmission was not severely degraded by ordered GB compared with that of perfect graphene and they attributed this degradation to the adsorbates²³. These previous theoretical works mainly concentrated on the transport direction across a single ordered GB but little involved with the transport direction along or with other angles relative to GB. The transport through the graphene with GBs should be direction-dependent due to the structure anisotropy of the system. Furthermore,

^a State Key Laboratory of Crystal Materials, Shandong University, 250100 Jinan, Shandong, PR China. Email: linnakth@gmail.com, zhaoxian@sdu.edu.cn.

^b Hefei National Laboratory for Physical Sciences at the Microscale, University of Science and Technology of China, Hefei 230026, China. Email: zyli@ustc.edu.cn.

^c Center for Bioengineering and Biotechnology, China University of Petroleum (East China), 266580 Qingdao, PR China.

* To whom correspondence should be addressed

false-color dark-field TEM (DF-TEM) image of polycrystalline graphene clearly displayed crossed GBs in samples¹¹. However, there is still no study on the electronic structure and transport properties of graphene with crossed GBs. A recent STM study also presented two identical GBs joined with a 120° turn²⁴. It is interesting the states existed in two GBs vanished at the 120° junction while its mechanism is still unknown.

Based on the unexplored issues mentioned above, in present study we carry out first principles calculations on the electronic structure and transport properties of graphene with GBs, in which four types of single GBs and two types of crossed GBs are taken into account. We consider the transport through the single GB with the directions including across and along the GB as well as other angles relative to the GB. We hope our calculations, to some extent, contribute to the design of practical electronic devices.

Computational details

For geometry structure relaxation and electronic structure calculations, we adopt first principles studies based on density functional theory (DFT) methods implemented in the SIESTA package²⁵. The generalized gradient approximation Perdew-Burke-Ernzerhof functional (GGA/PBE)²⁶ is used to describe exchange correlation with a mesh cutoff value of 200 Ry. Structural optimization is performed until the total force on each atom is less than 0.02 eV/Å. A vacuum layer larger than 15 Å is used to avoid interaction among periodic images. Based on the optimized structures, the electron transport properties are computed using nonequilibrium Green's function (NEGF) method implemented in TranSIESTA program²⁷. The left and right electrodes are chosen the same as the scattering region. The current through the system is calculated according to the Landauer – Büttiker formula:

$$I = G_0 \int T(E, V) [f_L(E) - f_R(E)] dE$$

where $G_0 = 2e^2/h$ is the unit of quantum conductance, $T(E, V)$ is the transmission coefficient at energy E and the bias voltage V , $f_L(E)$ and $f_R(E)$ are the Fermi distribution functions respectively at left and right electrodes. The local density approximation (LDA) is applied to compute the transport properties. The k -point samplings for the transmission spectra calculations are respectively 1, 100, and 100 in the x , y , z directions.

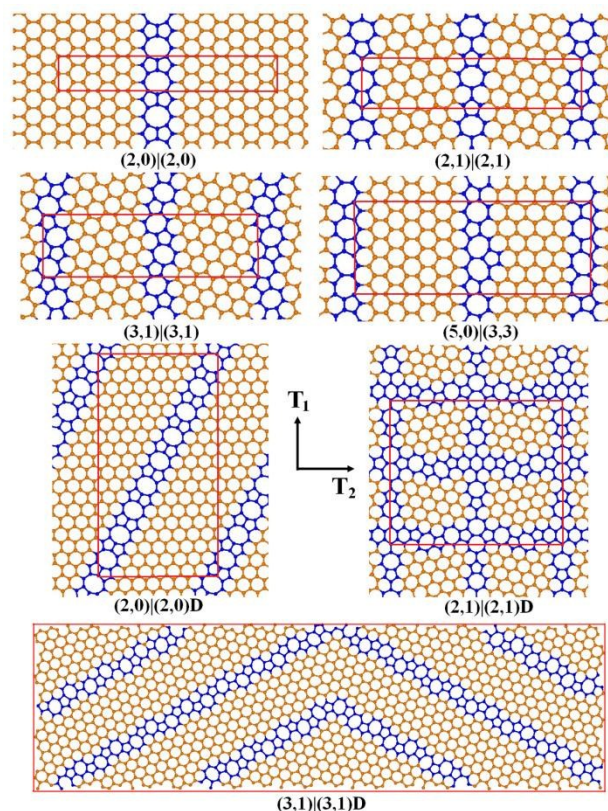


Figure 1. Atomic structure of graphene with GBs. The rectangular supercells used in this work depicted in red line.

GB structures

An ordered GB in graphene can be defined by two translation vectors (n_L, m_L) and (n_R, m_R) respectively belonging to the left and right crystal domains and oriented along the boundary line²⁰. The relationship between the translation vector and the GB structure has been proposed according to the arrangements of pentagons and heptagons on the boundary^{14, 28}. In the present study, we consider four typical single GBs, including three symmetric GBs, $(2,0)|(2,0)$, $(2,1)|(2,1)$, $(3,1)|(3,1)$ and an asymmetric GB, $(5,0)|(3,3)$, which were observed in experiment^{11, 29, 30} and widely investigated in theory³¹⁻³⁴. We also consider two crossed GBs $(2,1)|(2,1)D$ and $(3,1)|(3,1)D$, the latter has been found in a recent experiment²⁴. In addition, $(2,0)|(2,0)D$ GB is constructed to study the transport along a direction with a certain angle relative to GB. The method to satisfy periodic boundary of single ordered GBs has been proposed in Ref. 14. The periodic supercells of all studied GBs are shown in Figure 1.

Table 1. The supercell size of each GB.

	(2,0) (2,0)	(2,1) (2,1)	(3,1) (3,1)	(5,0) (3,3)	(2,0) (2,0)D	(2,1) (2,1)D	(3,1) (3,1)D
$T_1(\text{Å})$	4.9619	6.5939	8.9776	12.5622	39.3300	26.1572	35.9401
$T_2(\text{Å})$	31.4839	29.3414	31.1452	32.1596	21.0459	30.9972	124.6430

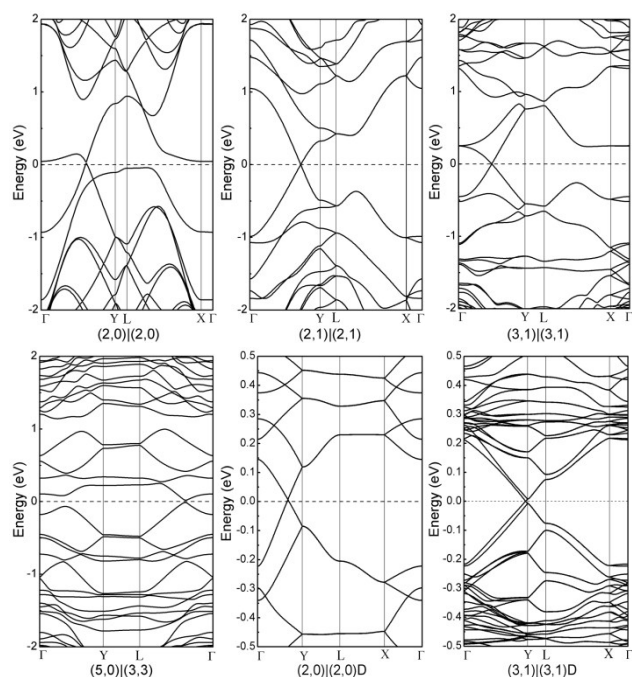


Figure 2. Band structure of graphene with GBs. The Fermi level is set to zero energy

The lattice vector (\mathbf{T}_1 , \mathbf{T}_2) values of rectangular cell are in Table 1. The direction of \mathbf{T}_1 and \mathbf{T}_2 is shown in Figure 1.

Results and Discussion

Calculations were carried out to examine the nature of the electronic bands introduced by GBs in graphene. The calculated results are displayed in Figure 2. For all GBs, a remarkable characteristic is that the zero band gap is not destroyed by embedded these ordered GBs in graphene, whereas a finite band gap has been found in graphene with Stone-Wales defects and dissociated pentagons and heptagons defects^{35, 36}. The Dirac point remains in our calculated band structure, however, its position lies not on the usual graphene Brillouin zone K point. The previous literature has shed light on the complex evolution of Dirac point toward GB with anisotropic Dirac cone³⁷.

In the case of (2,0)|(2,0) GB, it shows an almost flat band along the Γ -Y (L-X) line in the vicinity of Fermi level. The flat-band character is similar to that of the zigzag-edged graphene nanoribbons³⁸. In addition, the extended van Hove regions in the band structure of (2,0)|(2,0) GB are located at about ± 0.1 eV near the Fermi level. This phenomenon is confirmed by a recent experiment, which observed the van Hove singularity states were close to the Fermi energy in certain ordered GBs using scanning tunnelling microscopy¹⁶. These local band states also exist in (2,1)|(2,1) and (3,1)|(3,1) GB corresponding to the region within 0.5 eV below and above the Dirac point¹⁴. Similar to (2,0)|(2,0) GB, for the more

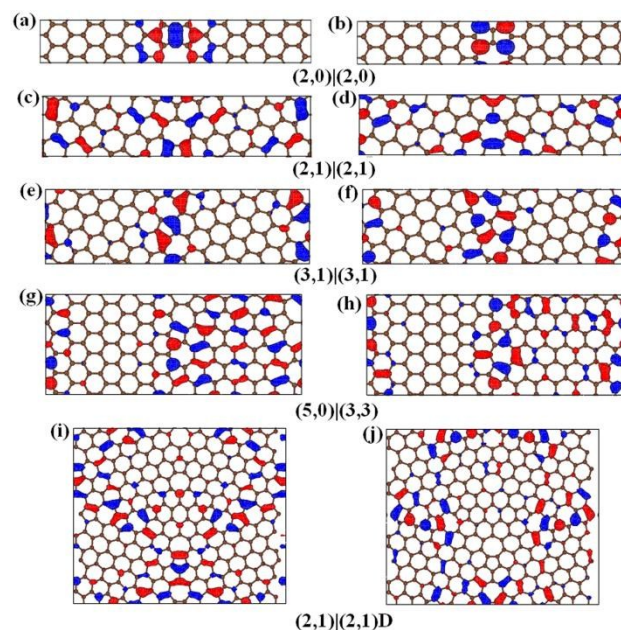


Figure 3. Wave functions of the highest valence band (left panels) and lowest conduction band (right panels) of each GBs. (2,0)|(2,0), (3,1)|(3,1), (5,0)|(3,3) at Γ points, (2,1)|(2,1), (2,1)|(2,1)D at Y points.

complex structure of (5,0)|(3,3) GB, there is also a flat band near the Fermi level.

We shift our focus now to the crossed GBs. The zero band gap nature is unexpected in the intersection of two GBs. The (2,1)|(2,1)D GB keeps the Dirac point on the Γ -Y line, nevertheless, the (3,1)|(3,1)D GB shifts to the Y point. A striking band-split along Γ -Y line is shown in (3,1)|(3,1)D GB. In addition, there is still a van Hove region around the L point in the vicinity of the Fermi level in the crossed GB (3,1)|(3,1)D.

In order to further investigate the properties of the band states lying close to the Fermi level, we represent isosurface contour plots of wave functions of the highest valence band (HVB) and lowest conduction band (LCB) at Γ point for (2,0)|(2,0), (3,1)|(3,1), (5,0)|(3,3) GBs and Y point for (2,1)|(2,1), (2,1)|(2,1)D GBs (see Figure 3). We can see that the states close to Fermi level are mainly localized along the GB region. For (2,0)|(2,0)GB, it shows the typical zigzag edge states found in zigzag nanoribbons. However, the GB states hybridized with the bulk states are found in (2,1)|(2,1) and (3,1)|(3,1) GB. These hybridized local states take place within a region of ~ 5 Å from the geometric center of the GB^{15, 16}. In the case of (5,0)|(3,3) GB, the asymmetric wave functions of both HVB and LCB show that some states in the armchair region are present in addition to the states in the GB region. As for the crossed GB (2,1)|(2,1)D, the localized states distribute along the GBs with the exception of the crossed region. Both the HVB and LCB states in the crossed region have a great difference with the states in other GB regions.

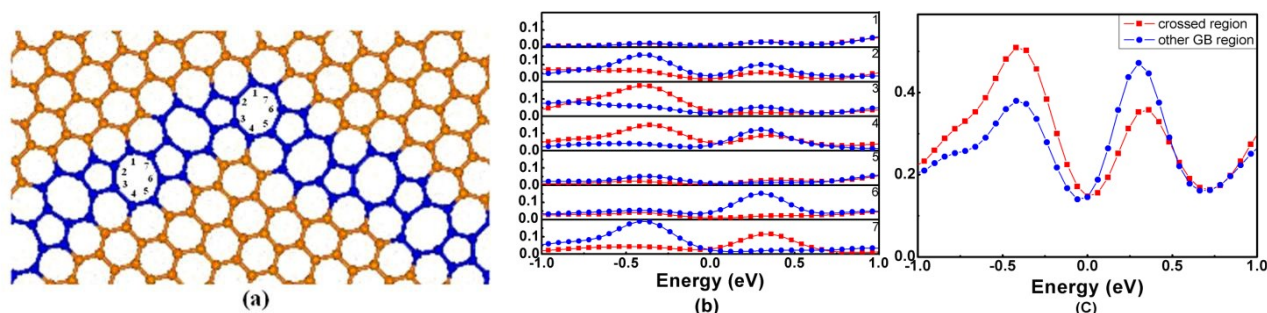


Figure 4. (a) Two heptagons in crossed region and other GB regions. The partial DOS, projected onto each atom (b) and heptagon core atoms (c), in two different regions.

The difference is probably due to the interaction of two GBs. Moreover, a recent experiment shows the states existed in two GBs vanished at the 120° junction in $(3,1)|(3,1)$ D GB²⁴.

To clarify the discrepancy of the electronic states in the crossed region and other GB regions, We project the total density of states (DOS) of $(3,1)|(3,1)$ D GB onto the carbon atoms, which belong to two heptagons, one in the crossed region and another in other GB regions (Figure 4 (a)). The partial DOS (PDOS) of the atoms and the heptagon core (sum over the PDOS of each atom) are shown in Figure 4(b) and 4(c), respectively. We can see that the heptagon in crossed region has a positive (negative) contribution to the total DOS below (above) the Fermi level compared with that in other GB regions. However, the PDOS of each atom shows more complex contribution in two different regions. For example, the atoms in position 1 and 5 in two regions have similar contribution to the total DOS, while large changes in other positions. In the case of the atom in position 6, we notice that a prominent peak in other GB region is located above the Fermi level but not in the

crossed region. This phenomenon is well agreement with the STM experimental observations²⁴.

In addition to the electronic structures, electronic transport across and along the single GBs are simulated by first principles quantum transport calculations based on density functional theory and the non-equilibrium Green's function formalism. The two-probe system has been adopted and a comparable size of the scattering region of each GB has been chosen in our calculations. The calculated zero-bias transmission spectra are collected in Figure 5. One can see that the transmission probabilities mainly decrease as the electrons across the GBs in the range of $|E| > 0.5\text{eV}$. This decreased transmission probabilities have also been found in other theoretical works^{20, 23}. However, an increased transmission intensity appears in the range of $|E| < 0.2\text{eV}$ of $(2,0)|(2,0)$ GB and $(5,0)|(3,3)$ GB and $|E| < 0.5\text{eV}$ of $(2,1)|(2,1)$ GB and $(3,1)|(3,1)$ GB. This is probably due to the existence of extended van Hove band states in this energy region, as shown in our calculated band structures, which has been verified to enhance the conductance around ordered grain boundaries¹⁶.

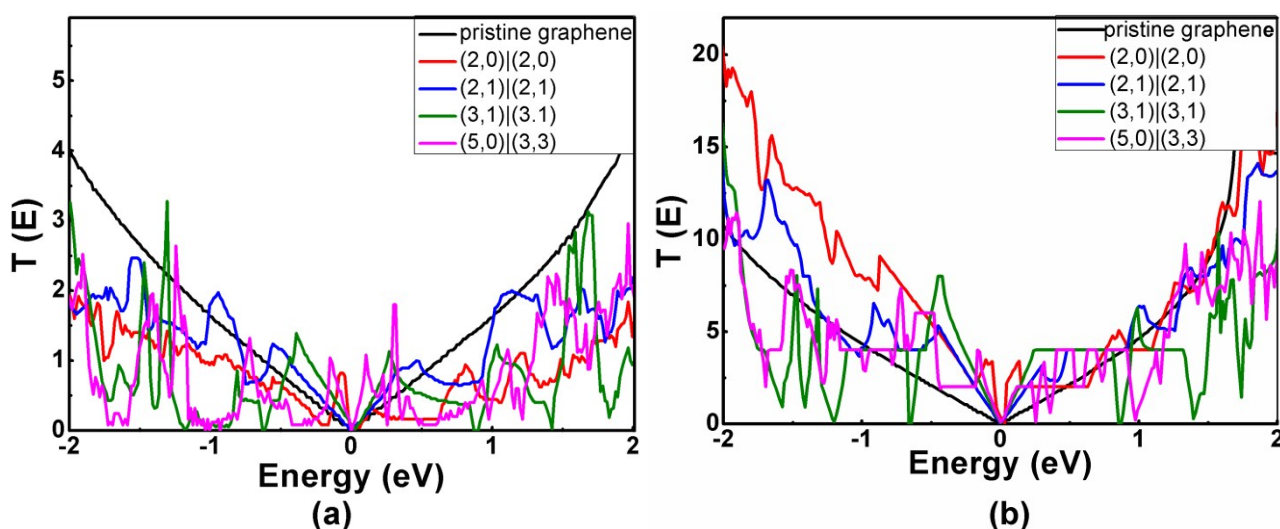


Figure 5. The transmission spectra at zero-bias. (a) transport across the GBs (b) transport along the GBs.

Comparison of the transmission spectra of these GBs, it is worth to stress that (2,1)|(2,1) GB has less effect to impede the electronic transport compared with other GBs. On the other hand, a distinct transport gap located at about -1.0eV is induced by (3,1)|(3,1) and (5,0)|(3,3) GBs. Therefore, the electronic transport properties depend on the specific GB structures. However, the GB structure is nubilous as the electronic transport properties measured in experiment^{13,17}. We consider this is the origin of the debate about whether the GB largely degrades the electronic transport.

It can be argued that our calculated transmission spectra are not consistent with that in other literatures. Take (5,0)|(3,3) GB as an example, a transport gap was found near the Fermi level by Yazyev and Louie²⁰, while not present in our result. We have repeated their result and attributed this discrepancy to the different electrode (we use the graphene with GB and they used the graphene without GB) applied in the calculations.

In sharp contrast to the transport across the GBs, the transmission probabilities along the GBs are not degraded.

Especially for (2,0)|(2,0) GB, which has been regarded as a good type of embedded metallic wire²⁹, presents strong transmission intense in the electrons region. Moreover, we still could clearly see the contribution of the extended van Hove band states to the transmission along the GB.

In addition to the zero-bias transmission spectra, we have also calculated the current-voltage (I-V) characteristics of the transport across and along the GBs, the calculated results are summarized in Figure 6 (a) and (b), respectively. As for the transport across the GBs, the declining currents induced by GBs correspond well with the zero-bias transmission analysis. We have noticed that the currents are suppressed at least by 50% compared with the pristine graphene, even up to 80% for (3,1)|(3,1) GB and (5,0)|(3,3) GB at about $E > 0.5\text{eV}$. Our results are much lower compared with other theoretical predicts which found the conductance of a GB would be nearly 70-80% of the bulk graphene conductance^{20,23}. In the case of the transport along the GBs, there is no large current decline compared with the transport across the GBs. For

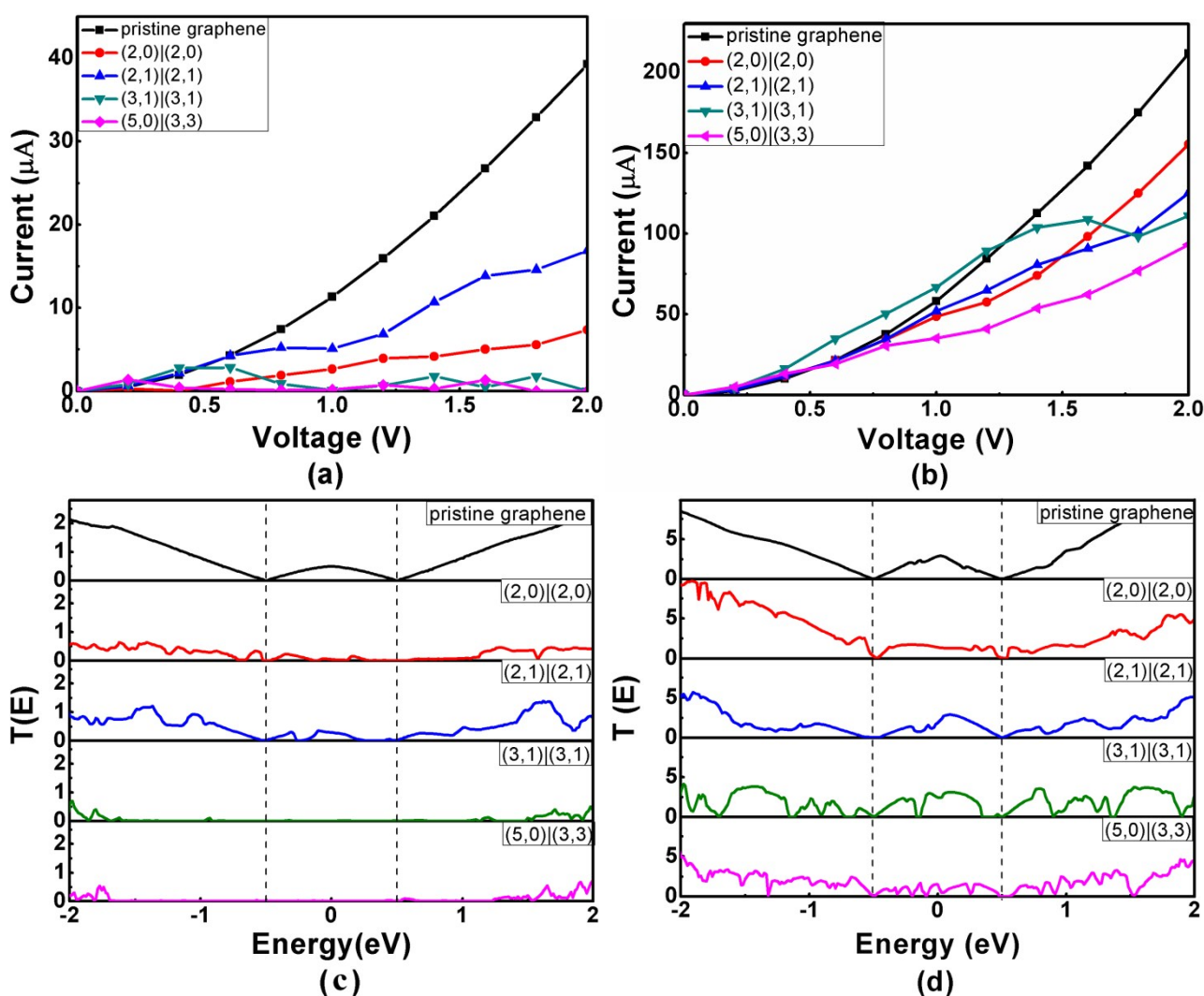


Figure 6. The current-voltage (I-V) characteristics and the transmission spectra at 1.0 V. (a),(c) transport across the GBs. (b), (d) transport along the GBs. The dashed line indicate the bias window.

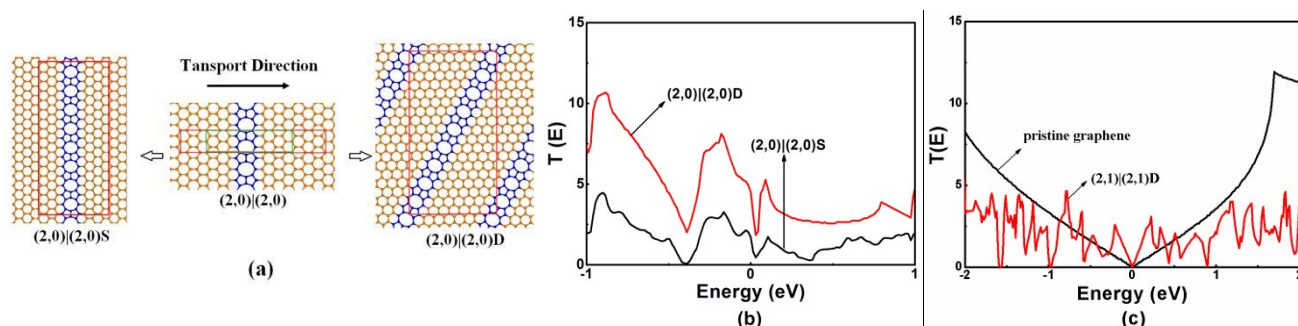


Figure 7. (a) $(2,0)|(2,0)D$ structure transform from the green rectangular supercell $(2,0)|(2,0)$ GB used to calculate the transport along other direction, $(2,0)|(2,0)S$ used to compare, the red rectangular supercell is the initial $(2,0)|(2,0)GB$. (b) The zero-bias transmission spectra of $(2,0)|(2,0)S$ and $(2,0)|(2,0)D$. (c) The zero-bias transmission spectra of crossed GB.

example, the reduction of current along the GB in asymmetric $(5,0)|(3,3)$ GB, which is the largest current decline in all GBs, is about half of the pristine graphene, while it is still much smaller than that across the GB. We also notice that the current along the GB is larger than that across the GB. This property is also revealed by previous experimental results¹³, which displayed the resistance of the inter-grain (across the GB) was larger than that of the intra-grain (along the grain) by using four-probe measurement. The anisotropic transport properties of graphene with GBs originate from its anisotropic electronic band structures³⁹ (see Figure 2). For all the structures we study here, both the top of the valence bands and the bottom of the conduction bands have much more significant dispersions along the $\Gamma - Y$ direction, which is along GB in the real space, however, these bands are more flat along the $\Gamma - X$ direction, which is across GB direction in the real space. Therefore, the corresponding effective mass of electrons and holes is also anisotropic because it is proportional to the inverse of the curvature of the band dispersion. This directly leads to the anisotropic $I - V$ curve and the associated resistance.

To gain further understanding of the current suppression, we have analysed the bias-dependent transmission spectra (Figure 6(c) and (d)). Here, we only plot the two directions transmission spectra at 1.0 V bias as an example. It is well known that the current is mainly attributed to the transmission coefficient around the Fermi level within the bias window. We have noticed that a large transport gap exists in $(3,1)|(3,1)$ and $(5,0)|(3,3)$ GB, respectively, which has no contribution to the current across the GBs. However, such a transport gap is not found in the transport along the GBs.

From the above discussions, we can at least conclude that the transport properties of graphene with GBs not only depend on the specific atomic GB structure, but also on the transport direction. Besides the transport across and along the GB, the case of the transport direction with a certain angle relative to $(2,0)|(2,0)$ GB has been investigated. To satisfy our calculation ability, a reduced supercell unit is employed to construct $(2,0)|(2,0)D$ and $(2,0)|(2,0)S$ system (Figure 7 (a)). $(2,0)|(2,0)D$ GB can be obtained by making a certain angle rotation from $(2,0)|(2,0)S$. The reduced supercell can not avoid period GB image interaction, which

introduces the states in Fermi level, but this interaction will not affect the main conclusion for the comparison of transport properties. The zero-bias transmission spectra of these two systems are shown in Figure 7(b). One can see that the electron transmission probabilities have been enlarged by avoiding transport across the GB. Although the full transport-direction relationship is not given, we still think it is a useful method to design more efficient electronic device based on graphene material with GBs by altering transport direction.

In the following part, we pay our attention to the transport of crossed GB $(2,1)|(2,1)D$, which contains two GB square crossing with each other. The transport direction is along one GB but across another. The zero-bias transmission spectrum is shown in Figure 7 (c). We notice that the transmission probabilities are decreased in the whole region except at $|E| < 0.5\text{eV}$, which is similar to the transport across a single GB. This indicates the GB vertical to the transport direction plays an important role in electronic transmission reduction. Moreover, the interaction of two GBs may not have great impact on the electronic transport properties compared with the presence of only single GB. Investigation of the crossed GB with other angles is outside the scope of our paper, nevertheless the significance of crossed GBs on the transport properties is demonstrated by compared with pristine graphene.

Conclusions

In summary, we have investigated the electronic structure and transport properties of graphene with GBs based on the density functional theory (DFT) combined with Green's functions technique. The presence of GBs does not destroy the zero band gap nature but leads to the occurrence of localized states near the Fermi level. Our transport calculations indicate that these states contribute to improve the electron transmission probabilities. The transport properties depend on the specific GB structures as well as the transport direction by comparing the zero-bias transmission spectra. The current at finite bias largely degrades as transport across the GB, while not large current reduction as transport along the GB. The transport along a direction with certain angles relative to GB also shows an increased electron

transmission probabilities compared with the transport across the GB. The transmission behavior of crossed GB is similar to the transport across a single GB. Our results show that the tailoring electronic transport by selecting transport direction through the GBs may be a useful method to design practical electronic devices based on graphene at realistic nanometre scale.

Acknowledgements

We acknowledge the National Nature Science Foundation of Shandong Province (Grant No.ZR2015BQ001), the General Financial Grant from the China Postdoctoral Science Foundation (Grant No.2013M531595) and the National Nature Science Foundation of China (Grant No. 21403300). The work was carried out at National Supercomputer Center in Tianjin, and the calculations were performed on TianHe-1(A). The authors also acknowledge a generous grant of computer time from the Norwegian Programme for Supercomputing.

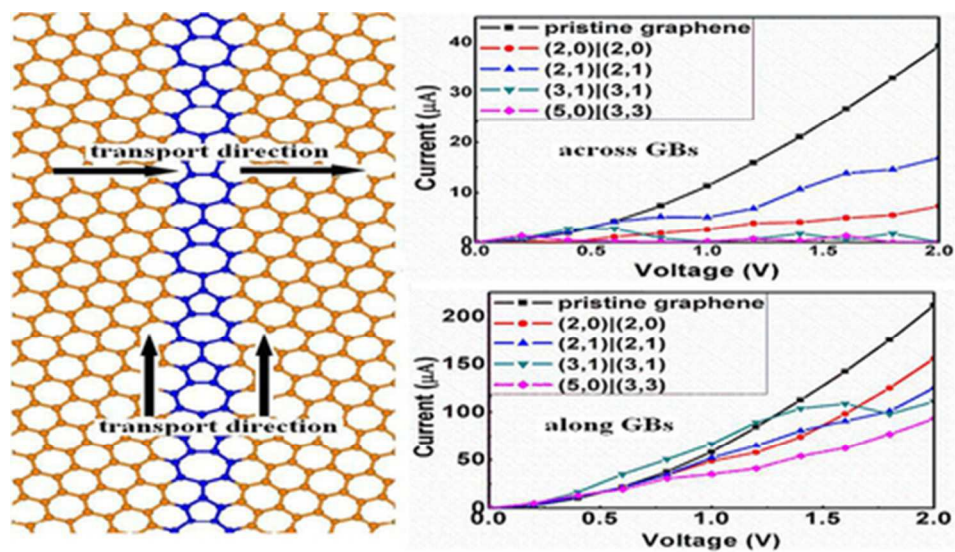
References

1. K. S. Novoselov, A. K. Geim, S. V. Morozov, D. Jiang, Y. Zhang, S. V. Dubonos, I. V. Grigorieva and A. A. Firsov, *Science*, 2004, **306**, 666-669.
2. A. K. Geim and K. S. NOVOSELOV, *Nature Mater*, 2007, **6**, 183-191.
3. A. H. Castro Neto, F. Guinea, N. M. R. Peres, K. S. Novoselov and A. K. Geim, *Rev. Mod. Phys.*, 2009, **81**, 109-162.
4. Shuaihua Ji, J. B. Hannon, R. M. Tromp, V. Perebeinos, J. Tersoff and F. M. Ross, *Nature Mater*, 2012, **11**, 114-119.
5. Hao Ren, Qunxiang Li, Yi Luo, and Jinlong Yang, *Appl. Phys. Lett.*, 2009, **94**, 173110.
6. G. M. Rutter, J. N. Crain, N. P. Guisinger, T. Li, P. N. First and J. A. Stroscio, *Science*, 2007, **317**, 219-222.
7. Xuesong Li, Weiwei Cai, Jinho An, Seyoung Kim, Junghyo Nah, Dongxing Yang, Richard Piner, Aruna Velamakanni, Inhwa Jung, Emanuel Tutuc, Sanjay K. Banerjee, Luigi Colombo and Rodney S. Ruoff, *Science*, 2009, **324**, 1312-1314.
8. Jinho An, Edgar Veolkl, Ji Won Suk, Xuesong Li, Carl W. Magnuson, Lianfeng Fu, Peter Tiemeijer, Maarten Bischoff, Bert Freitag, Elmira Popova, and Rodney S. Ruoff, *Nano Lett.*, 2011, **5**, 2433-2439.
9. Dinh Loc Duong, Gang Hee Han, Seung Mi Lee, Fethullah Gunes, Eun Sung Kim, Sung Tae Kim, Heetae Kim, Quang Huy Ta, Kang Pyo So, Seok Jun Yoon, Seung Jin Chae, Young Woo Jo, Min Ho Park, Sang Hoon Chae, Seong Chu Lim, Jae Young Choi and Young Hee Lee, *Nature*, 2012, **490**, 235-240.
10. Gwan-Hyoung Lee, Ryan C. Cooper, Sung Joo An, Sunwoo Lee, Arend van der Zande, Nicholas Petrone, Alexandra G. Hammerberg, Changgu Lee, Bryan Crawford, Warren Oliver, Jeffrey W. Kysar and James Hone, *Science*, 2013, **340**, 1073-1076.
11. Kwanpyo Kim, Zonghoon Lee, William Regan, C. Kisielowski, M. F. Crommie and A. Zettl, *Nano Lett.*, 2011, **5**, 2142-2146.
12. Junfeng Zhang, Jijun Zhao and Jianping Lu, *Nano Lett.*, 2012, **6**, 2704-2711.
13. Qingkai Yu, Luis A. Jauregui Wei Wu, Robert Colby, Jifa Tian, Zhihua Su, Helin Cao, Zhihong Liu, Deepak Pandey, Dongguang Wei, Ting Fung Chung, Peng Peng, Nathan P. Guisinger, Eric A. Stach, Jiming Bao, Shin-Shem Pei and Yong P. Chen, *Nature Mater*, 2011, **10**, 443-449.
14. Oleg V. Yazyev and Steven G. Louie, *Phys. Rev. B*, 2010, **81**, 195420.
15. Simone S. Alexandre, A. D. Lúcio, A. H. Castro Neto and R. W. Nunes, *Nano Lett.*, 2012, **12**, 5097-5012.
16. Chuanxu Ma, Haifeng Sun, Yeliang Zhao, Bin Li, Qunxiang Li, Aidi Zhao, Xiaoping Wang, Yi Luo, Jinlong Yang, Bing Wang, and J. G. Hou, *Phys. Rev. Lett.*, 2014, **112**, 226802.
17. Pinshane Y. Huang, Carlos S. Ruiz-Vargas, Arend M. van der Zande, William S. Whitney, Mark P. Levendorf, Joshua W. Kevek, Shivank Garg, Jonathan S. Alden, Caleb J. Hustedt, Ye Zhu, Jiwoong Park, Paul L. McEuen and David A. Muller, *Nature*, 2011, **496**, 389-393.
18. Kendal W. Clark, X-G. Zhang, Ivan V. Vlassiouk, Guowei He, Randall M. Feenstra and An-Ping Li, *ACS Nano*, 2013, **7**, 7956-7966.
19. Haider I. Rasool, Colin Ophus, William S. Klug, A. Zettl and James K. Gimzewski, *Nat. Commun*, 2013, **4**, 2811.
20. Oleg V. Yazyev and Steven G. Louie, *Nature Mater*, 2010, **9**, 806-809.
21. Junfeng Zhang, Junfeng Gao, Lizhao Liu and Jijun Zhao, *J. Appl. Phys.*, 2012, **112**, 053713.
22. Péter Vancsó, Gézal. Márk, Philippe Lambin, Alexandre Mayer, Yong-Sung Kim, Chanyong Hwang and László P. Biro, *CARBON*, 2013, **64**, 101-110.
23. Hengji Zhang, Geunsik Lee, Cheng Gong, Luigi Colombo, and Kyeongjae Cho, *J. Phys. Chem. C*, 2013, **118**, 2338-2343.
24. Y. Tison, Jérôme Lagoute, Vincent Repain, Cyril Chacon, Yann Girard, Frédéric Joucken, Robert Sporken, Fernando Gargiulo, Oleg V. Yazyev and Sylvie Rousset, *Nano Lett.*, 2014, **14**, 6382-6386.
25. José M Soler, Emilio, Julian D Gale, Alberto García, Javier Junquera, Pablo Ordejón and Daniel Sánchez-Portal, *J. Phys.: Condens. Matter*, 2002, **14**, 2745-2779.
26. John P. Perdew, Kieron Burke and Matthias Ernzerhof, *Phys. Rev. Lett.*, 1996, **77**, 3865-3868.
27. Mads Brandbyge, José-Luis Mozos, Pablo Ordejón, Jeremy Taylor and Kurt Stokbro, *Phys. Rev. B*, 2002, **65**, 165401.
28. Junfeng Zhang and Jijun Zhao, *CARBON*, 2013, **55**, 9.
29. Jayeeta Lahiri, You Lin, Pinar Bozkurt, Ivan I. Oleynik and Matthias Batzil, *Nature Nanotech.*, 2010, **5**, 326-329.
30. Bao Yang, Hai Xu, Jiong Lu, and Kian Ping Loh, *J. AM. CHEM. SOC.*, 2014, **136**, 12401-12406.
31. Yanyue Liu and Boris I. Yakobson, *Nano Lett.*, 2010, **10**, 2178-2183.
32. M. A. Akhukov, A. Fasolino, Y. N. Gornostyrev and M. I. Katsnelson, *Phys. Rev. B*, 2012, **85**, 115407
33. IaS. Bala Kumar and Jing Guo, *Nano Lett.*, 2012, **12**, 1362-1366.

ARTICLE

RSC Advances

34. Aron W. Cummings, Alessandro Cresti and Stephan Roche, *Phys.Rev. B*, 2014, **90**, 161401.
35. Joice da Silva-Araújo, H. Chacham and R. W. Nunes, *Phys.Rev. B*, 2010, **81**, 193405.
36. Sharmila N. Shirodkar and Umesh V. Waghmare, *Phys.Rev. B*, 2012, **86**, 165401.
37. Joice da Silva Araújo and R. W. Nunes, *Phys.Rev. B*, 2010, **81**, 043708.
38. Kyoko Nakada, Mitsutaka Fujita, Gene Dresselhaus and Mildred S. Dresselhaus, *Phys.Rev. B*, 1996, **54**, 24.
39. Liangzhi Kou, Thomas Frauenheim and Changfeng Chen, *J. Phys. Chem. Lett.*, 2014, **5**, 7.



39x22mm (300 x 300 DPI)